Electronic Supplementary Material (ESI) for ChemComm.


# From thiophosphate to chalcohalide: mixed-anion $AgS_xCl_y$ ligands concurrently enhancing nonlinear optical effect and laser-damage threshold

Lihua Gao,[‡a] Yu Chu,[‡b] Xiaowen Wu,[a] Bingbing Zhang,[a] Kui Wu*[,a]

[a]College of Chemistry and Environmental Science, Key Laboratory of Analytical Science and Technology of Hebei Province, Hebei University, Baoding, China

[b]Xinjiang Technical Institute of Physics & Chemistry, CAS; 40-1 South Beijing Road, Urumqi 830011, China

*To whom correspondence should be addressed :*

*E-mail: wukui@hbu.edu.cn (Kui Wu)*

## CONTENTS

## 1. Synthesis of $Ag_5PS_4Cl_2$

All the reagents ($Ag_2S$, AgCl, P, and S) with high purity (>99.9%) were directly purchased from the Beijing Hawk Technology Co., Ltd. $Ag_5PS_4Cl_2$ was synthesized with the stoichiometric ratio ($Ag_2S$: AgCl : P : S = 1.5 : 2 : 1: 2.5). We have firstly placed the raw materials into the graphite crucibles and then put the crucibles into the silicon tubes to eliminate the corrosion problem between quartz tube and raw materials. Then, quartz tubes were heated to be 550 °C in 20 h and kept at this temperature for about 50 h, slowly down to ambient temperature within 3 days. N, N−dimethylformamide (DMF) solvent was chosen to wash the products and many yellow microcrystals of $Ag_5PS_4Cl_2$ were found and stable in air after several months. In order to obtain the large particle-size single-crystals, the above polycrystalline samples were further sintered at 450 °C for ten days within a muffle furnace.

## 2. Structural Refinement and Crystal Data

Selected high-quality crystals were used for data collections on a Bruker SMART APEX II 4K CCD diffractometer using Mo Kα radiation (λ = 0.71073 Å) at 296 K. The crystal structures were solved by direct method and refined using the SHELXTL program package.[1] Multi-scan method was used for absorption correction.[2] Rational anisotropic thermal parameters for all atoms were obtained by the anisotropic refinement and extinction correction. PLATON was also used to check the final structures and no other symmetries were found.[3] Detail refinement parameters and data were shown in Table S1.

## 3. Property Characterization

### 3.1 Powder X-ray Diffraction

Powder X-ray diffraction (XRD) patterns of title compounds were collected on a Bruker D2 X-ray diffractometer with Cu Kα radiation (λ = 1.5418 Å) at room temperature. The $2\theta$ range was 10-70° with a step size of 0.02° and a fixed counting time of 1s/step.

### 3.2 UV−Vis−Near-IR (NIR) Diffuse-Reflectance Spectrum

Diffuse-reflectance spectra were measured by a Shimadzu SolidSpec-3700DUV spectrophotometer in the wavelength range of 200−1100 nm at room temperature.

### 3.3 Thermal analysis

A HCT-2 (HENVEN) thermal analyzer was used to investigate their differential scanning calorimetric (DSC) curves. About 5 mg microcrystals were placed into a vacuum-sealed silica tube (Φ4×2 $mm^3$). The measurement ranges are located at the temperature from 30 to 550 $^oC$. The temperature rates in heating and cooling process were 5 $^oC$/min, respectively.

### 3.4 Raman Spectroscopy

Hand-picked crystals were firstly put on an object slide, and then a LABRAM HR Evolution spectrometer equipped with a CCD detector by a 532 nm laser was used to record the Raman spectrum. The integration time was set to be 5 s.

### 3.5 Second-harmonic Generation Measurement

Through the Kurtz and Perry method,[4] powder SHG response was investigated by a Q-switch laser (2.09 μm, 3 Hz, 50 ns) with different particle sizes, including 38−55, 55−88, 88−105, 105−150, 150−200, and 200−250 μm. The $AgGaS_2$ crystal was ground and sieved into the same size range as the reference.

### 3.6 LDT Measurement

LDT was evaluated on powder sample (150−200 μm) with a pulsed YAG laser (1.06 μm, 10 ns, 10 Hz). Similar size of $AgGaS_2$ is chosen as the reference. The judgment criterion is as follows: with increasing laser energy, the color change of the powder sample is constantly observed by optical microscope to determine the damage threshold. To adjust different laser beams, an optical concave lens is added into the laser path. The damage spot is measured by the scale of optical microscope.

### 3.7 Computational Description

Crystal orbital Hamilton population (COHP) calculations were computed using the LMTO package, the original basis set and its basic functions (s, p, d, and f) manage to reconstruct the PAW electronic structure. −ICOHP values were calculated by integrating over all filled states to give relative overlap populations.

The Gaussian 09 package was employed to explore the electronic structures of $AgS_xCl_y$ anionic groups at molecular level. DFT method at the B3LYP level with

DGDZVP basis sets was performed to calculate the cluster.

In order to further investigate the relationship of structure–property, the electronic structure of $Ag_5PS_4Cl_2$ was studied by density functional theory (DFT) calculation.[5] The exchange-correlation potential was calculated using Perdew–Burke–Ernzerhof (PBE) functional within the generalized gradient approximation (GGA) with the scheme.[6] The following orbital electrons were treated as valence electrons, Ag: $4p^6$ $4d^{10}$ $5s^1$, P: $3s^2$ $3p^3$, S: $3s^2$ $3p^4$, Cl: $3s^2$ $3p^5$. To achieve energy convergence, a plane-wave basis set energy cutoff was 720 eV within normal-conserving pseudo-potential (NCP).[7] As important parameters for NLO crystal, SHG coefficient and refractive index were also calculated.[8] Owing to the discontinuity of exchange correlation energy, the experimental value is usually larger than that of calculated band gap. Thus, scissors operator is used to make the conduction band agree with the experimental value.

## 4. Figures and Tables

**Table S1.** Crystal data and structure refinement for $Ag_5PS_4Cl_2$.

**Table S2.** Coordination environment of Ag atoms in the $AgS_xCl_y$-based quaternary chalcohalides without disordered structures.

**Table S3.** LDTs of $Ag_5PS_4Cl_2$ and $AgGaS_2$ (as the reference).

**Table S4**. Calculated dipole moments (Debye) of anionic groups ($AgS_2Cl_2$, $AgS_3Cl_2$ and $PS_4$) in $Ag_5PS_4Cl_2$.

**Table S5.** Performance comparison between $Ag_5PS_4Cl_2$, $Ag_3PS_4$ and $AgGaS_2$ (as the reference) including AGS as the $AgGaS_2$, $E_g$ as the bandgap, $d_{ij}$ as the calculated NLO coefficient.

**Fig. S1** (a) Structural types of $AgS_4$, $AgS_5$, $AgS_2Cl_2$, $AgS_3Cl_2$; (b) hyperpolarizability ($|\beta_{max}|$); (c) HOMO−LUMO gap ($E_g$, eV); (d) polarizability anisotropy (δ).

**Fig. S2** (left) COHP curves for Ag-S and Ag-Cl bond; (right) –ICOHP (eV/bond) values of Ag-S and Ag-Cl in $Ag_5PS_4Cl_2$.

**Fig. S3** Powder XRD patterns of $Ag_5PS_4Cl_2$.

**Fig. S4** Raman spectrum of $Ag_5PS_4Cl_2$.

**Fig. S5** Birefringence curve of $Ag_5PS_4Cl_2$.

**Table S1.** Crystal data and structure refinement for $Ag_5PS_4Cl_2$.

| Empirical formula | $Ag_5PS_4Cl_2$ |
|---|---|
| formula weight | 769.46 |
| crystal system | *Orthorhombic* |
| space group | *Amm*2 |
| cell parameter *a* (Å) | 7.44(3) |
| cell parameter *b* (Å) | 11.17(4) |
| cell parameter *c* (Å) | 6.30(2) |
| Z, *V* (Å$^3$) (Volume) | 2, 524(3) |
| $D_c$ (g/cm$^3$) (calculated density) | 4.877 |
| μ (mm$^{-1}$) (absorption coefficient) | 10.571 |
| goodness-of-fit on $F^2$ | 1.179 |
| $R_1$, $wR_2$ ($I > 2\sigma(I)$)[a] | 0.0513, 0.1515 |
| $R_1$, $wR_2$ (all data) | 0.0623, 0.1697 |
| Flack factor | 0.07(19) |
| largest diff. peak and hole (e·Å$^{-3}$) | 1.532, −1.939 |

[a] $R_1 = F_o - F_c / F_o$ and $wR_2 = [w (F_o^2 - F_c^2)^2 / wF_o^4]^{1/2}$ for $F_o^2 > 2\sigma (F_o^2)$

**Table S2.** Coordination environment of Ag atoms in the $AgS_xCl_y$-based quaternary chalcohalides without disordered structures.

| | Space group | $AgS_xCl_y$ ligands |
|---|---|---|
| $Ag_2Bi_2S_3Cl_2$ | *P*-1 | $AgS_4Cl_2$ |
| $Ag_6GeS_4Cl_2$ | *Pnma* | $AgS_2Cl_3$, $AgS_3Cl_2$, $AgS_2Cl_2$, $AgS_4Cl_2$ |
| $AgBi_2S_2Cl_3$ | *C*2/*m* | $AgS_2Cl_4$ |
| $AgBiCl_2S$ | *Cmcm* | $AgS_2Cl_4$ |
| $Ag_{15}(PS_4)_4Cl_3$ | *I*-43*d* | $AgS_3Cl$ |
| $Ag_5PS_4Cl_2$ | *Amm*2 | $AgS_3Cl_2$, $AgS_2Cl_2$, |

**Table S3.** LDTs of $Ag_5PS_4Cl_2$ and $AgGaS_2$ (as the reference).

| compounds | damage energy (mJ) | spot diameter (mm) | LDT (MW/cm$^2$) | LDT (× AGS)* |
|---|---|---|---|---|
| $AgGaS_2$ | 0.58 | 0.5 | 29.6 | 1 |
| $Ag_5PS_4Cl_2$ | 2.20 | 0.5 | 112.5 | 3.8 |

*AGS = $AgGaS_2$

**Table S4**. Calculated Dipole Moments (Debye) of anionic groups ($AgS_2Cl_2$, $AgS_3Cl_2$, and $PS_4$) in $Ag_5PS_4Cl_2$.

| | $Ag_5PS_4Cl_2$ | | | |
|---|---|---|---|---|
| | *x* | *y* | *z* | dipole moment (debye) |
| $AgS_2Cl_2$ | 0 | 0 | 0.31 | 0.31 |
| $AgS_3Cl_2$ | 0 | 0 | 3.72 | 3.72 |
| $PS_4$ | 0 | 0 | 7.73 | 7.73 |
| **Total** | 0 | 0 | 11.75 | 11.75 |

**Table S5.** Performance comparison between $Ag_5PS_4Cl_2$, $Ag_3PS_4$ and $AgGaS_2$ (as the reference) including AGS as the $AgGaS_2$, $E_g$ as the bandgap, $d_{ij}$ as the calculated NLO coefficient.

| Compounds | $Ag_5PS_4Cl_2$ | $Ag_3PS_4$[9] | $AgGaS_2$[10,11] |
|---|---|---|---|
| Space group | *Amm*2 | *Pmn*2$_1$ | *I*-42*d* |
| $E_{g(exp.)}/E_{g(cal.)}$ (eV) | 2.71/1.2 | 2.43/1.14 | 2.64 |
| Powder $d_{ij(exp.)}$ (×AGS) | 2.5 | 1.3 | 1.0 |
| Maximum $d_{ij(cal.)}$ (pm/V) | 22.7 | 15.8 | 13.0 |
| LDT (× AGS) | 3.8 | ~1.0 | 1.0 |
| $\Delta n$@1.06μm | 0.171 | 0.065 | 0.039 |

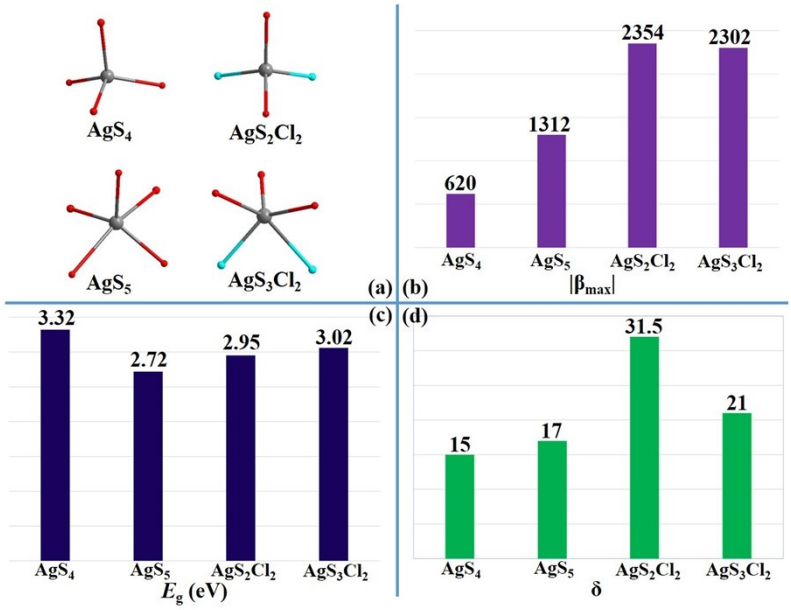


**Fig. S1** (a) Structural types of $AgS_4$, $AgS_5$, $AgS_2Cl_2$, $AgS_3Cl_2$; (b) hyperpolarizability ($|\beta_{max}|$); (c) HOMO−LUMO gap ($E_g$, eV); (d) polarizability anisotropy (δ).

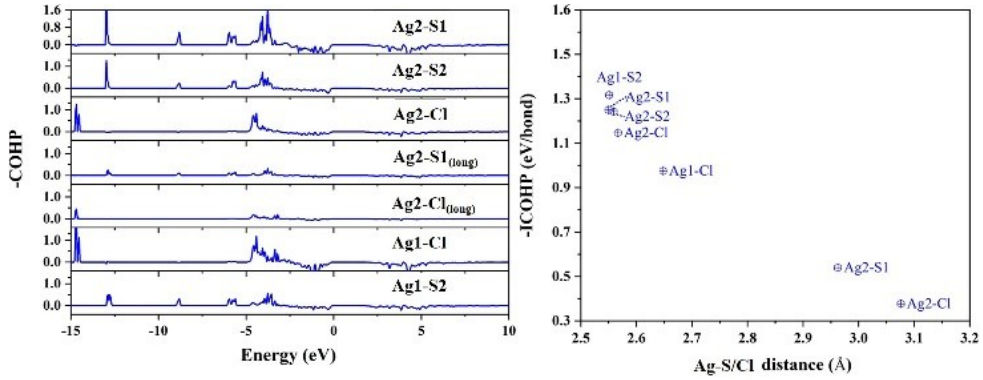


**Fig. S2** (left) COHP curves for Ag-S and Ag-Cl bond; (right) –ICOHP (eV/bond) values of Ag-S and Ag-Cl in $Ag_5PS_4Cl_2$.

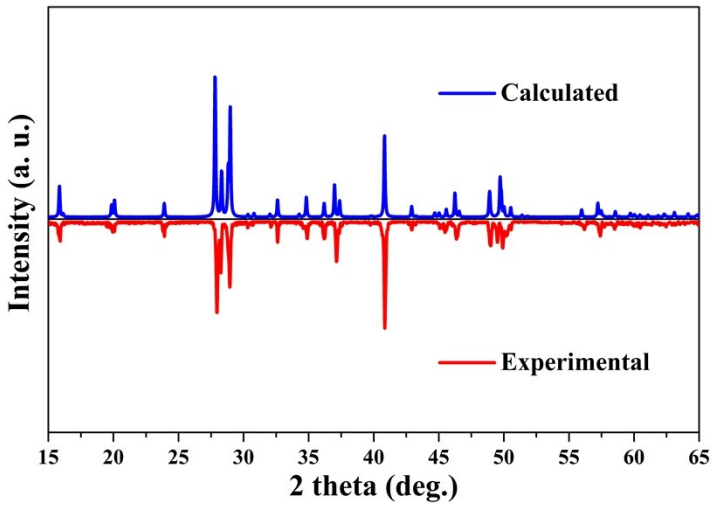


**Fig. S3** Powder XRD patterns of $Ag_5PS_4Cl_2$.

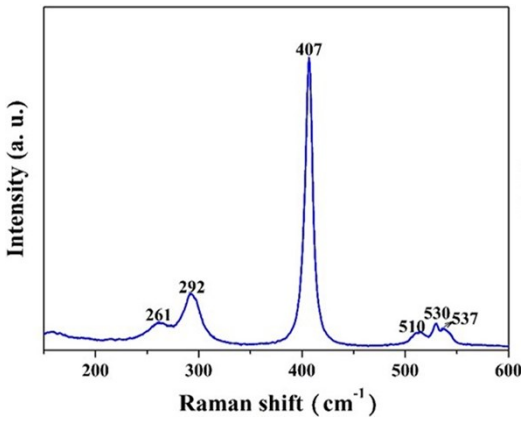


**Fig. S4** Raman spectrum of $Ag_5PS_4Cl_2$.

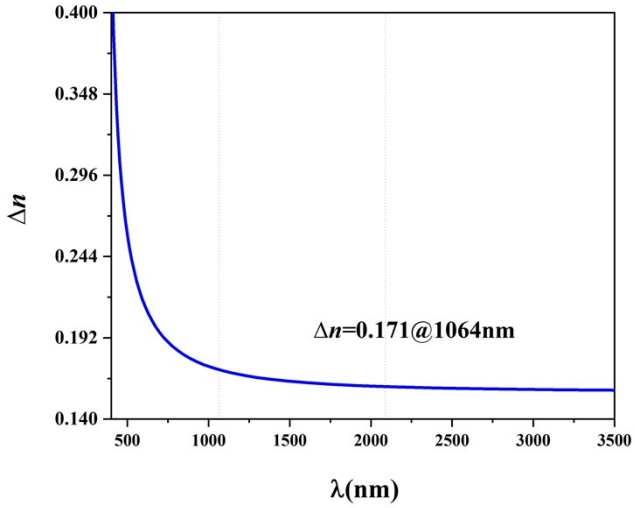


**Fig. S5** Birefringence curve of $Ag_5PS_4Cl_2$.

## 5. References


1 *SAINT*, version 7.60A; Bruker Analytical X-ray Instruments, Inc.: Madison, WI, 2008.

2 G. M. Sheldrick, *SHELXTL*, version 6.14; Bruker Analytical Xray Instruments, Inc.: Madison, WI, 2003.

3 A. L. Spek, *J. Appl. Crystallogr.,* 2003, **36**, 7.

4 S. K. Kurtz and T. T. Perry, *J. Appl. Phys.,* 1968, **39**, 3798.

5 S. J. Clark, M. D. Segall, C. J. Pickard, P. J. Hasnip, M. J. Probert, K. Refson and M. C. Payne, *Z. Kristallogr.,* 2005, **220**, 567.

6 J. P. Perdew, K. Burke and M. Ernzerhof, *Phys. Rev. Lett.,* 1996, **77**, 3865.

7 A. M. Rappe, K. M. Rabe, E. Kaxiras and J. D. Joannopoulos, *Phys. Rev. B,* 1990, **41**, 1227.

8 R. W. Godby, M. Schluter and L. J. Sham, *Phys. Rev. B: Condens. Matter Mater. Phys.,* 1988, **37**, 10159.

9 Y. Yang, B. B. Zhang, X. W. Wu and K. Wu, *Dalton Trans.*, 2021, 10.1039/D1DT00366F.

10 L. Isaenko, I. Vasilyeva, A. Merkulov, A. Yelisseyev and S. Lobanov, *J. Cryst. Growth,* 2005, **275**, 217;

11 L. Isaenko and I. Vasilyeva, *J. Cryst. Growth,* 2008, **310**, 1954.